Atmos. Chem. Phys. Discuss., 13, 14037–14067, 2013
www.atmos-chem-phys-discuss.net/13/14037/2013/
doi:10.5194/acpd-13-14037-2013

Atmospheric Chemistry and Physics Discussions

An evaluation of the CMAQ reproducibility of satellite tropospheric NO_2 column observations at different local times over East Asia

H. Irie[1], K. Yamaji[2], K. Ikeda[2], I. Uno[3], S. Itahashi[4], T. Ohara[5], and J. Kurokawa[6]

[1]Center for Environmental Remote Sensing, Chiba University, 1-33 Yayoicho, Inage-ku, Chiba 263-8522, Japan
[2]Research Institute for Global Change, Japan Agency for Marine-Earth Science and Technology, 3173-25 Showa-machi, Kanazawa-ku, Yokohama, Kanagawa 236-0001, Japan
[3]Research Institute for Applied Mechanics, Kyushu University, 6-1 Kasuga Park, Kasuga, Fukuoka 816-8580, Japan
[4]Department of Earth System Science and Technology, Kyushu University, 6-1 Kasuga Park, Kasuga, Fukuoka 816-8580, Japan
[5]National Institute for Environmental Studies, 16-2 Onogawa, Tsukuba, Ibaraki 305-8506, Japan
[6]Asia Center for Air Pollution Research, 1182 Sowa, Nishi-ku, Niigata 950-2144, Japan

Received: 22 March 2013 – Accepted: 13 May 2013 – Published: 28 May 2013

Correspondence to: H. Irie (hitoshi.irie@chiba-u.jp)

Published by Copernicus Publications on behalf of the European Geosciences Union.

Abstract

Despite the importance of the role of nitrogen dioxide (NO_2) in tropospheric chemistry, the causes leading to the discrepancy between satellite-derived and modeled tropospheric NO_2 vertical column densities (VCDs) over East Asia remain unclear. Here the reproducibility of satellite tropospheric NO_2 VCD data by a regional chemical transport model (CMAQ) with the Regional Emission inventory in ASia (REAS) Version 2 is evaluated from the viewpoint of the diurnal variation of tropospheric NO_2 VCDs, where satellite observations at different local times (SCIAMACHY/ENVISAT, OMI/Aura, and GOME-2/Metop-A) are utilized considering literature validation results. As a case study, we concentrate on June and December 2007 for a detailed evaluation based on various sensitivity simulations, for example with different spatial resolutions (80, 40, 20, and 10 km) for CMAQ. For June, CMAQ generally reproduces absolute values of satellite NO_2 VCDs and their diurnal variations over all 12 selected diagnostic regions in East Asia. In contrast, a difficulty arises in interpreting the significant disagreement between satellite and CMAQ values over most of the diagnostic regions in December. The disagreement cannot be explained by any of the sensitivity simulations performed in this study. To address this, more investigations, including further efforts for satellite validations in wintertime, are needed.

1 Introduction

Accurate modeling of atmospheric chemistry is needed for the current understanding and future prediction of the atmospheric environment from the perspectives of not only air quality but also climate. In recent years, East Asian countries are recognized to have brought a continuous increase in the emissions of nitrogen oxides ($NO_x = NO + NO_2$) (e.g., Ohara et al., 2007), which play a central role in tropospheric chemistry. Thus, an evaluation of the ability of NO_x simulations in East Asia can provide us with a critical constraint for improving atmospheric chemistry modeling. On regional to global scales,

van Noije et al. (2006) compared tropospheric NO_2 vertical column densities (VCDs) from 17 different international global atmospheric chemistry models with observations from the GOME (Global Ozone Monitoring Experiment) satellite instrument and found that the models tend to underestimate the satellite data in industrial regions, especially over Central Eastern China (CEC). Over the same region, GOME tropospheric NO_2 VCDs were compared with those simulated by the Community Multi-scale Air Quality (CMAQ) model using the Regional Emission inventory in Asia (REAS) Version 1 (Ohara et al., 2007), showing an underestimation by the model (Uno et al., 2007). The identified underestimation was then attributed mainly to the limited accuracy of basic energy statistical data, emission factors, and socio-economic data used to construct the emission inventory. Han et al. (2009) also studied GOME vs. CMAQ comparisons using the 2001 ACE-ASIA (Asia Pacific Regional Aerosol Characterization Experiment) emission inventory and found a large discrepancy between GOME and CMAQ tropospheric NO_2 VCDs in fall and winter. In particular, the CMAQ tropospheric NO_2 VCDs were low by $\sim 57.3\,\%$ over North China. In these ways, absolute values of tropospheric NO_2 VCDs, derived from a single set of satellite data, have been mainly discussed so far, limiting discussion of other aspects, such as the diurnal variation.

In recent years until April 2012, three different satellite sensors, SCIAMACHY (SCanning Imaging Absorption Spectrometer for Atmospheric CHartographY) (Bovensmann et al., 1999), OMI (Ozone Monitoring Instrument) (Levelt et al., 2006), and GOME-2 (Callies et al., 2000), were all in orbit together, observing tropospheric NO_2 VCDs on a global scale. Observations by these satellite sensors were performed at different local times, and the diurnal variation pattern seen in the NO_2 data has been reported for various locations over the world (Boersma et al., 2008). For their validation, Irie et al. (2012) used ground-based Multi-Axis Differential Optical Absorption Spectroscopy (MAX-DOAS) observations performed at several sites in Japan and China in 2006–2011. Utilizing the ability of MAX-DOAS to provide continuous measurements during daytime, these data were used as a common reference to validate all three

satellite data sets and it was concluded that biases between satellite and MAX-DOAS VCDs are insignificant for SCIAMACHY, OMI, and GOME-2.

Here the present work considers the validation results from Irie et al. (2012) and evaluates the reproducibility of satellite tropospheric NO_2 VCD data by the chemical transport model CMAQ, from the viewpoint of the diurnal variation of tropospheric NO_2 VCDs. For CMAQ simulations, we use the REAS Version 2 emission inventory (Kurokawa et al., 2013). Various sensitivity simulations, for example at different spatial resolutions (80, 40, 20, and 10 km), are examined for a detailed evaluation.

2 CMAQ

The present study evaluates CMAQ Version 4.7.1 (Byun and Schere, 2006), which is driven by meteorological fields generated by the WRF (Weather Research and Forecasting) Version 3.3 model (Skamarock and Klemp, 2008) with 2007 NCEP (National Centers for Environmental Prediction) Final Analysis data (ds083.2). We use the SAPRC-99 (Statewide Air Pollution Research Center-99) gas-phase atmospheric chemical mechanisms with 72 chemical species and 214 chemical reactions and 30 photochemical reactions for the gas-phase chemistry. The aerosol module AERO5 (Carlton et al., 2010) is used for aerosols. Cloud and aqueous chemistry and dry deposition are represented by the Asymmetric Convective Model (ACM) cloud processor using the ACM methodology to compute convective mixing. For the advection, the piecewise parabolic method (Colella and Woodward, 1984) is employed. ACM version 2 (ACM2) vertical diffusion instrumented for in-line calculation of emissions is used for the turbulent diffusion. The lateral boundary conditions are taken from monthly mean values calculated by the CHemical AGCM for Study of atmospheric Environment and Radiative forcing (CHASER) (Sudo et al., 2002). We use default profiles as initial conditions and the first 30 days are treated as a spin up period.

As anthropogenic emissions over East Asia, we adopt the REAS Version 2 data (Kurokawa et al., 2013). Biomass burning and biogenic emission data are taken from

the Reanalysis of the Tropospheric chemical composition over the past 40 yr (RETRO, http://retro.enes.org) and the Model of emissions of gases and aerosols from nature Version 2.0 (MEGAN Version 2.0, http://acd.ucar.edu/~guenther), respectively.

For the sensitivity simulations, we test 4 different horizontal resolutions of 80 (as the base case), 40, 20, and 10 km (Table 1), which result in grid cell numbers of 95 × 75, 110 × 88, 184 × 132, and 292 × 182, respectively. A one-way nesting method is adopted for each inner domain simulation. The corresponding domains are shown in Fig. 1. We also test the sensitivity of soil NO_x emission by running models with or without it (Table 1). As other sensitivity tests, we change the emission strength by ±20 % over the whole of the model domain. This number is chosen as an increase or decrease by 20 % can roughly compensate differences found between wintertime tropospheric NO_2 VCDs from CMAQ base case simulations and satellite observations over CEC, as shown later. Additional sensitivity tests are performed in vertical layers that are represented by 37 or 14 sigma–pressure coordinated layers from the surface to 50 hPa with the first layer height being around 20 m. Also, the impact of reducing the emission injection height by half and the impact of the diurnal variation of emissions are investigated assuming a diurnal variation pattern that was best estimated by Lin et al. (2010). In this diurnal variation pattern, the ratio of hourly emissions to the daily mean has a minimum at ∼ 0.6 (at 00:00–04:00 LT) and maximum at ∼ 1.2 (at 09:00–19:00 LT).

We set the model to output data every 1 h for each simulation. For all grids, the model values are interpolated over time to estimate tropospheric NO_2 VCDs at local times of satellite observations.

3 Satellite data

In this work, tropospheric NO_2 VCD data from SCIAMACHY, OMI, and GOME-2 are utilized together. SCIAMACHY onboard the ENVISAT satellite was launched in March 2002. It passes over the equator at about 10:00 LT. Its global coverage observations are

performed in six days, with a spatial resolution of $60 \times 30\,km^2$. OMI onboard the Aura satellite was launched in July 2004. Its equator crossing time is about 13:40–13:50 LT. Global coverage is achieved daily at a nominal nadir spatial resolution of $13 \times 24\,km^2$. GOME-2 was launched onboard a MetOp satellite in June 2006. A ground-pixel size is usually $80 \times 40\,km^2$ ($240 \times 40\,km^2$ for the back scan). An equator crossing time is around 09:30 LT. Global coverage is achieved every day. While observations by these three sensors are thus performed with somewhat different specifications, the present study attempts to use their tropospheric NO_2 VCD data together by using the products retrieved with the same basic algorithm (DOMINO products for OMI and TM4NO2A products for SCIAMACHY and GOME-2) (Boersma et al., 2004, 2007, 2011). For polluted situations, the error in the satellite tropospheric NO_2 VCD data was estimated to be $\sim 1 \times 10^{15}\,molecules\,cm^{-2}$ + 30 %, including uncertainties in the slant column, the stratospheric column, and the tropospheric air mass factor (AMF) (Boersma et al., 2004). In the present study, comparisons with CMAQ are made for the Version 2 retrievals under cloud-free conditions, i.e. cloud fraction (CF) less than 20 %. To estimate the biases in the SCIAMACHY, OMI, and GOME-2 tropospheric NO_2 VCD data in a consistent manner, Irie et al. (2012) used a single data set from ground-based MAX-DOAS observations performed at three sites in Japan and three sites in China in 2006–2011. From their regression analysis between satellite and MAX-DOAS tropospheric NO_2 VCDs, it was concluded that the biases with respect to MAX-DOAS values are less than about 10 % and insignificant for all three data sets. It should be noted that their bias estimates are based mainly on the comparisons made around summer (May, June, and September) over China. This is discussed later to better interpret the differences seen in comparisons between NO_2 VCDs from satellite observations and CMAQ calculations in the present study.

4 Comparisons

Here, comparisons are performed focusing on June and December 2007. As a case study, only these two months are examined in the present study, because the computational cost for CMAQ simulations under various conditions, particularly with fine horizontal resolution, is huge. The year 2007 was chosen considering that (1) the period covered by GOME-2, SCIAMACHY, and OMI at the same time was 2007–2012 and (2) an earlier time would be better, in general, for a lesser chance of satellite instrument degradation and the availability of more mature emission inventories. Concentrating on these two months, model evaluations were performed for 12 selected diagnostic regions, which are defined as in Fig. 1. In the figure, the 12 diagnostic regions are drawn with rectangles on CMAQ-simulated NO_2 fields with different spatial resolutions of 80, 40, 20, and 10 km. Latitude and longitude ranges for each region are given in Table 2.

While various horizontal resolutions are mixed among data sets from not only the CMAQ simulations but also the satellite observations, the 12 diagnostic regions have been selected to be wider than any horizontal resolutions, in order to discuss satellite vs. CMAQ comparisons under conditions with a similar spatial representativeness over the area of interest. Also, to increase the representativeness over time as well, monthly-mean tropospheric NO_2 VCDs from satellite observations and CMAQ simulations are compared for each of the 12 diagnostic regions. Satellite-based monthly-mean tropospheric NO_2 VCDs were estimated from swath data with a cloud fraction less than 20 % to ensure moderate quality and a sufficient number of data points. The estimated monthly-mean VCDs can be different from the true monthly-mean values due to the lack of NO_2 VCDs under cloudy conditions. To investigate its impact, monthly-mean NO_2 VCDs were calculated using various cloud fraction thresholds. In Fig. 2, satellite-based tropospheric NO_2 VCDs are plotted against the cloud fraction threshold over the CEC region. The largest difference of NO_2 VCDs with respect to the value at a cloud fraction of 20 % is found to be ~ 30 %, which is much smaller than the quoted uncertainty in the satellite retrievals, as discussed later. It is interesting to note that the de-

pendence on the cloud fraction threshold for June is not as significant as for December. Also, a similar diurnal variation pattern, particularly as the difference between morning and afternoon values, can be seen even using different cloud fraction thresholds. The same characteristics were seen for the other diagnostic regions (not shown). Thus, below we assume that diurnal variations (differences between morning and afternoon values) seen from satellite observations are reliable, particularly in June.

4.1 Results for June 2007

In Fig. 3, monthly-mean tropospheric NO_2 VCDs from satellite observations are plotted in pink as a function of local time for the CEC, NCP, BEI, and SCN regions in June 2007. The associated error bars represent simple averages of quoted uncertainties in the satellite swath data used for monthly-mean calculations. Their magnitudes are much larger than the range (with respect to the value at a cloud fraction of 20 %, as mentioned above) of NO_2 VCDs at different cloud fraction thresholds (Fig. 2). As seen from Fig. 3, the NO_2 VCD tends to increase from 09:30 (GOME-2) to 10:00 LT (SCIAMACHY). This tendency is consistent with that seen from MAX-DOAS observations at Beijing in summers of 2008–2011 (Ma et al., 2013) but different from MAX-DOAS observations showing a decrease of NO_2 VCD from 09:30 to 10:00 LT around the center of CEC (Tai'an) in June 2006 (Irie et al., 2008) and around Beijing in summers of 2008–2012 (Hendrick et al., 2013). Detailed validation comparisons using MAX-DOAS observations at several locations in Japan and China were conducted by Irie et al. (2012) and it was concluded that biases for GOME-2 and SCIAMACHY data are likely insignificant, with the most probable estimates of biases of $+1 \pm 14$ % and -5 ± 14 %, respectively. Assuming their results that GOME-2 data have a positive bias and SCIAMACHY data have a negative bias enlarges the tendency found in Fig. 3 and therefore enlarges the difference from the tendency reported by Irie et al. (2008) and Hendrick et al. (2013). We should note, however, that uncertainties in both SCIAMACHY and GOME-2 data are much larger than the difference between GOME-2 and SCIAMACHY values, as seen in Fig. 3. Considering that the difference is likely to be insignificant, the present

study focuses only on larger differences that occur between afternoon and morning values. The afternoon values observed by OMI are smaller than the morning values derived from GOME-2 and SCIAMACHY. This tendency is consistent with all the above-mentioned MAX-DOAS observations performed by Irie et al. (2008), Ma et al. (2013), and Hendrick et al. (2013).

Several lines without error bars in Fig. 3 are tropospheric NO_2 VCDs simulated by CMAQ. Thick, solid black lines are for CMAQ base case simulations with a horizontal resolution of 80 km. Other black lines show results from simulations at horizontal resolutions of 40, 20, and 10 km. The ratio of CMAQ-simulated tropospheric NO_2 VCDs at horizontal resolutions of 10 and 80 km (R) is given for each simulation in Table 3. It can be seen from Fig. 3 and Table 3 that the CMAQ NO_2 VCD increases, when the horizontal resolution is improved from 80 to 10 km. This can be interpreted as the pronounced effects of the nonlinearity of chemistry (Valin et al., 2011) over given model grids, where NO_x emissions have to be artificially distributed. It is interesting to note that for CEC, NCP, and SCN the magnitude of such effects brought by improving horizontal resolutions can be as large as that caused by increasing emissions by 20 %, as shown by black lines with triangles (Fig. 3). A 20 % decrease (increase) in emissions leads to a 21–22 % decrease (a 23–24 % increase) in NO_2 VCDs for CEC. The impact on NO_2 VCDs by the same amount of emission changes is larger for December, as mentioned later. For BEI, the R value is as large as 1.48–2.06 (Table 3) and the impact of the change in horizontal resolution is larger than that of an emission change by 20 %. As discussed later, this also occurs in December and for the PRD, JPN, and KOR regions in both June and December. These regions, including BEI, are characterized by strong emissions occurring in a limited space. The R values over these regions are larger than those over the other regions. The R value is usually larger at 13:45 than at 09:30–10:00, probably reflecting effects of the nonlinearity of chemistry, which should be OH-dependent.

Results for the other sensitivity simulations are also shown in Fig. 3. When the number of layers is reduced from 37 (black; base case simulations) to 14 (sky blue), the

changes in NO_2 VCDs are negligibly small. When the injection height is reduced by half (purple), NO_2 VCDs tend to increase but only small changes take place. The omission of soil NO_x emissions (orange crosses) leads to a significant reduction of NO_2 VCD in June. Considering diurnal variation of emissions, the morning and afternoon NO_2 VCD values decrease and increase, respectively. This does not always produce better agreement with diurnal variation patterns seen from satellite measurements.

In Fig. 4, comparisons for the YTD, PRD, JPN, and KOR regions are shown. General characteristics of the comparisons for the YTD region are similar to those for CEC, NCP, BEI, and SCN (Fig. 3). For the PRD region, the CMAQ base run values show significant underestimation, where the values are out of the error ranges for both GOME-2 and SCIAMACHY NO_2 VCD data. An increase in emissions by 20 % or an improvement of the spatial resolution (from 80 to 20 km) leads to greater NO_2 VCDs in the model, but either of the two alone is insufficient in explaining the satellite NO_2 VCDs. It can be seen that NO_2 VCDs at a 20 km resolution exceed the values for the 20 % increase in the emissions. This is because the source regions influencing NO_2 VCD over PRD are limited, and we expect greater NO_2 VCDs at improved spatial resolutions over 20 km.

Of all the 12 selected diagnostic regions, comparisons for JPN show the best agreement. This may support that the REAS Version 2 emission inventory around JPN estimated based on the Japan Auto-Oil Program (JATOP; Kurokawa et al., 2013) is reliable. For JPN and KOR, the impact of spatial resolution is large, similar to those for PRD and BEI regions as mentioned above.

Figure 5 shows comparisons over 4 marine regions. All CMAQ simulations conducted for the marine regions show agreement with satellite observations to within their error range. It is worthwhile to mention here that tropospheric NO_2 VCDs can vary with different horizontal resolutions, probably due to effects of the nonlinearity of chemistry (Valin et al., 2011), where ship emissions might be significant enough to drive the effect. Or, a contamination might occur due to an intensified penetration of high-NO_2 air masses from land at finer horizontal resolutions, as discussed in detail later on.

In summary, for June 2007, diurnal variation patterns (differences between morning and afternoon values) are reproduced well by CMAQ for all 12 diagnostic regions. Quantitative agreement can also be given, when potential influences of CMAQ horizontal resolution and uncertainty in the satellite data are taken into account.

4.2 Results for December 2007

For December 2007, comparisons for all 12 diagnostic regions are shown in Figs. 6, 7, and 8, in manners similar to Figs. 3, 4, and 5 for June 2007. For the CEC, NCP, BEI, and SCN regions, it can be seen that diurnal variation patterns differ between satellite and CMAQ NO_2 VCD values (Fig. 6). As given in Table 4, over CEC, for example, the satellite data indicate that the afternoon-to-morning ratios of VCDs are about 0.6 in both June and December, whereas CMAQ indicates ratios of 0.7 and 1.0 in June and December, respectively (Table 5). In general, since the photochemical activity in winter is weaker than in summer, it is reasonable to expect a larger afternoon-to-morning ratio in winter than in summer, with a smaller amplitude of the NO_2 diurnal variation or even a larger NO_2 VCD in the afternoon than in the morning. Similar features were reported by Cede et al. (2006) for NO_2 column measurements in Maryland, USA and by Ma et al. (2013) and Hendrick et al. (2013) for MAX-DOAS measurements around Beijing, China. According to simulations by Uno et al. (2007), the NO_2 chemical lifetime estimated from the chemical reaction term reveals a longer lifetime in December (about 12–72 h) than in June (about 6 h) in the lower troposphere. This expected variation is calculated by CMAQ but not seen from satellite data (Fig. 6 and Tables 4 and 5). CMAQ data better agree with or overestimate satellite data in the afternoon, whereas CMAQ tends to underestimate satellite data (GOME-2 and SCIAMACHY) in the morning. The same tendency is seen for the other years (Itahashi et al., 2013). Also, this is consistent with the results of Han et al. (2011), who have also shown a significant disagreement between diurnal variation patterns from model and satellite data.

To explain the difference seen in Fig. 6 from the viewpoint of the uncertainty in emissions, we may need for emissions to increase in the morning and to decrease in the

afternoon. However, simulations assuming the diurnal variation pattern derived by Lin et al. (2010) (green crosses in Fig. 6) indicate that its sensitivity is too small to explain. None of the sensitivity simulations in the present study show a significant improvement in the slope of NO_2 VCDs between morning and afternoon.

From the sensitivity simulations, we quantify impacts by a simple change in the emission strength on NO_2 VCD values. A decrease (increase) in emissions by 20 % leads to a 35–36 % decrease (a 39–41 % increase) in NO_2 VCDs for CEC. These magnitudes are much larger than that found in June (Fig. 3).

For YTD, PRD, JPN, and KOR, both morning and afternoon CMAQ data agree with satellite values to within the error ranges (Fig. 7). Comparisons for marine regions (ECS, SOJ, SCS, and SJP) show a tendency that the CMAQ data are larger than satellite values (Fig. 8). This is evident in SOJ, where the differences cannot be explained by any sensitivity simulations or satellite data uncertainty. In SOJ, there are some negative values in the satellite swath data. These may suggest that the subtraction of the stratospheric NO_2 column from the total NO_2 in the satellite retrieval procedure had a difficulty in winter, when the stratospheric NO_2 is usually more abundant compared to the summer.

It is noted here that even over the ocean, NO_2 VCD increases as the spatial resolution is improved (Fig. 8 and Table 3). Compared to SOJ, this effect is large in ECS, SCS, and SJP, where ship emissions could be significant. It is thought that the increase occurs partly because of the nonlinear chemistry over these regions, where the spatial scale for NO_x emission from ships is small enough. Also, at finer spatial resolutions, vertical transport of NO_x by convection is more suppressed (Wild et al., 2006), potentially enhancing NO_2 VCDs.

The R values in December are usually similar to or smaller than those in June over all 12 diagnostic regions, except for ECS, SCS, and SJP (Table 3). The three regions are close to the eastern coast of China, where a penetration of high-NO_2 air masses from China is more visible at finer horizontal resolutions in Fig. 1. Thus, it is likely

that a contamination by such high-NO_2 air masses occurs, enhancing R values at fine resolutions over ECS, SCS, and SJP in December.

As discussed above, we have faced a difficulty in interpreting a significant disagreement between satellite and CMAQ values in December. The present study has assumed so far that the satellite data can be used to derive diurnal variation patterns based on validation comparison results (Irie et al., 2012). In the validation comparisons done by Irie et al. (2012), however, the results were mostly based on comparisons with ground-based MAX-DOAS measurements performed in months other than December. Taking this fact into consideration, efforts for satellite validation seem insufficient and therefore we suggest further precise validation study to identify the cause of differences, especially for the wintertime.

5 Conclusions

To evaluate the CMAQ reproducibility of satellite-retrieved tropospheric NO_2 VCD data over East Asia, we utilized SCIAMACHY, OMI, and GOME-2 data to realize comparisons from the viewpoint of the diurnal variation of NO_2. Various sensitivity simulations were conducted using CMAQ for detailed comparisons. The comparisons have been made focusing on 12 diagnostic regions (Fig. 1) and the two months of June and December 2007. In June 2007, diurnal variation patterns (differences between morning and afternoon values) were well reproduced by CMAQ for all 12 diagnostic regions. Quantitative agreement was also found, when potential influences of CMAQ horizontal resolutions and uncertainty in satellite data were taken into account. Over Central Eastern China (CEC), for example, the afternoon-to-morning ratios of VCDs derived from satellite and CMAQ data are about 0.6 and 0.7, respectively. For the Beijing (BEI), Pearl River Delta (PRD), Japan (JPN), and Korean (KOR) regions, where strong emissions occur in a limited space, large impacts of spatial resolution on NO_2 simulations were seen compared to the other regions. Comparisons for JPN show the best agreement, supporting the accuracy of the REAS Version 2 emission inventory, at

least around JPN. In contrast, a difficulty arises in interpreting comparisons between satellite and CMAQ values over most of the diagnostic regions in December. For CEC, the afternoon-to-morning ratios of VCDs from satellite and CMAQ are about 0.6 and 1.0, respectively. The disagreement cannot be explained by any sensitivity simulations performed in this study. To address this, more investigations, including further efforts for satellite validation, particularly in wintertime, are needed.

Acknowledgements. This work was supported by the Global Environment Research Fund (S-7) of the Ministry of the Environment, Japan. We acknowledge the free use of tropospheric NO_2 column data from www.temis.nl.

References

Boersma, K. F., Eskes, H. J., and Brinksma, E. J.: Error analysis for tropospheric NO_2 retrieval from space, J. Geophys. Res., 109, D04311, doi:10.1029/2003JD003962, 2004.

Boersma, K. F., Eskes, H. J., Veefkind, J. P., Brinksma, E. J., van der A, R. J., Sneep, M., van den Oord, G. H. J., Levelt, P. F., Stammes, P., Gleason, J. F., and Bucsela, E. J.: Near-real time retrieval of tropospheric NO_2 from OMI, Atmos. Chem. Phys., 7, 2103–2118, doi:10.5194/acp-7-2103-2007, 2007.

Boersma, K. F., Jacob, D. J., Eskes, H. J., Pinder, R. W., Wang, J., and van der A, R. J.: Intercomparison of SCIAMACHY and OMI tropospheric NO_2 columns: observing the diurnal evolution of chemistry and emissions from space, J. Geophys. Res., 113, D16S26, doi:10.1029/2007JD008816, 2008.

Boersma, K. F., Eskes, H. J., Dirksen, R. J., van der A, R. J., Veefkind, J. P., Stammes, P., Huijnen, V., Kleipool, Q. L., Sneep, M., Claas, J., Leitão, J., Richter, A., Zhou, Y., and Brunner, D.: An improved tropospheric NO_2 column retrieval algorithm for the Ozone Monitoring Instrument, Atmos. Meas. Tech., 4, 1905–1928, doi:10.5194/amt-4-1905-2011, 2011.

Bovensmann, H., Burrows, J. P., Buchwitz, M., Frerick, J., Noel, S., Rozanov, V. V., Chance, K. V., and Goede, A. H. P.: SCIAMACHY – mission objectives and measurement modes, J. Atmos. Sci., 56, 127–150, 1999.

Byun, D. W. and Schere, K. L.: Review of the governing equations, computational algorithm, and other components of the Models-3 Community Multi-scale Air Quality (CMAQ) Modeling system, Appl. Mech. Rev., 59, 51–77, 2006.

Callies, J., Corpaccioli, E., Eisinger, M., Hahne, A., and Lefebvre, A.: GOME-2- Metop's second-generation sensor for operational ozone monitoring, ESA Bull., 102, 28–36, 2000.

Carlton, A. G., Bhave, P. V., Napelenok, S. L., Edney, E. O., Sarwar, G., Pinder, R. W., Pouliot, G. A., and Houyoux, M.: Model representation of secondary organic aerosol in CMAQv4.7, Environ. Sci. Technol., 44, 8553–8560, 2010.

Cede, A., Herman. J., Richter, A., Krotkov, N., and Burrows, J.: Measurements of nitrogen dioxide total column amounts using Brewer double spectrophotometer in direct Sun mode, J. Geophys. Res., 111, D05304, doi:10.1029/2005JD006585, 2006.

Colella, P. and Woodward, P. R.: The piecewise parabolic method (PPM) for gas dynamical simulations, J. Comp. Phys., 54, 174–201, 1984.

Han, K. M., Song, C. H., Ahn, H. J., Park, R. S., Woo, J. H., Lee, C. K., Richter, A., Burrows, J. P., Kim, J. Y., and Hong, J. H.: Investigation of NO_x emissions and NO_x-related chemistry in East Asia using CMAQ-predicted and GOME-derived NO_2 columns, Atmos. Chem. Phys., 9, 1017–1036, doi:10.5194/acp-9-1017-2009, 2009.

Han, K. M., Lee, C. K., Lee, J., Kim, J., and Song, C. H.: A comparison study between model-predicted and OMI-retrieved tropospheric NO_2 columns over the Korean peninsula, Atmos. Environ., 45, 2962–2971, 2011.

Hendrick, F., Müller, J.-F., Clémer, K., De Mazière, M., Fayt, C., Hermans, C., Stavrakou, T., Vlemmix, T., Wang, P., and Van Roozendael, M.: Four years of ground-based MAX-DOAS observations of HONO and NO_2 in the Beijing area, Atmos. Chem. Phys. Discuss., 13, 10621–10660, doi:10.5194/acpd-13-10621-2013, 2013.

Irie, H., Kanaya, Y., Akimoto, H., Tanimoto, H., Wang, Z., Gleason, J. F., and Bucsela, E. J.: Validation of OMI tropospheric NO_2 column data using MAX-DOAS measurements deep inside the North China Plain in June 2006: Mount Tai Experiment 2006, Atmos. Chem. Phys., 8, 6577–6586, doi:10.5194/acp-8-6577-2008, 2008.

Irie, H., Boersma, K. F., Kanaya, Y., Takashima, H., Pan, X., and Wang, Z. F.: Quantitative bias estimates for tropospheric NO_2 columns retrieved from SCIAMACHY, OMI, and GOME-2 using a common standard for East Asia, Atmos. Meas. Tech., 5, 2403–2411, doi:10.5194/amt-5-2403-2012, 2012.

Itahashi, S., Uno, I., Irie, H., Kurokawa, J., and Ohara, T.: Trend analysis of tropospheric NO_2 column density over East Asia during 2000–2010: multi-satellite observations and model simulations with the updated REAS emission inventory, Atmos. Chem. Phys. Discuss., 13, 11247–11268, doi:10.5194/acpd-13-11247-2013, 2013.

Kurokawa, J., Ohara, T., Morikawa, T., Hanayama, S., Greet, J.-M., Fukui, T., Kawashima, K., and Akimoto, H.: Emissions of air pollutants and greenhouse gases over Asian regions during 2000–2008: Regional Emission inventory in ASia (REAS) version 2, Atmos. Chem. Phys. Discuss., 13, 10049–10123, doi:10.5194/acpd-13-10049-2013, 2013.

Levelt, P. F., van den Oord, G. H. J., Dobber, M. R., Malkki, A., Visser, H., de Vries, J., Stammes, P., Lundell, J., and Saari, H.: The Ozone Monitoring Instrument, IEEE T. Geosci. Remote, 44, 5, 1093–1101, doi:10.1109/TGRS.2006.872333, 2006.

Lin, J.-T., McElroy, M. B., and Boersma, K. F.: Constraint of anthropogenic NO_x emissions in China from different sectors: a new methodology using multiple satellite retrievals, Atmos. Chem. Phys., 10, 63–78, doi:10.5194/acp-10-63-2010, 2010.

Ma, J. Z., Beirle, S., Jin, J. L., Shaiganfar, R., Yan, P., and Wagner, T.: Tropospheric NO_2 vertical column densities over Beijing: results of the first three years of ground-based MAX-DOAS measurements (2008–2011) and satellite validation, Atmos. Chem. Phys., 13, 1547–1567, doi:10.5194/acp-13-1547-2013, 2013.

Ohara, T., Akimoto, H., Kurokawa, J., Horii, N., Yamaji, K., Yan, X., and Hayasaka, T.: An Asian emission inventory of anthropogenic emission sources for the period 1980–2020, Atmos. Chem. Phys., 7, 4419–4444, doi:10.5194/acp-7-4419-2007, 2007.

Skamarock, W. C. and Klemp, J. B.: A time-split nonhydrostatic atmospheric model for weather research and forecasting applications, J. Comput. Phys., 227, 3465–3485, 2008.

Sudo, K., Takahashi, M., Kurokawa, J., and Akimoto, H.: CHASER: a global chemical model of the troposphere 1. Model description, J. Geophys. Res., 107, 4339, doi:10.1029/2001JD001113, 2002.

Uno, I., He, Y., Ohara, T., Yamaji, K., Kurokawa, J.-I., Katayama, M., Wang, Z., Noguchi, K., Hayashida, S., Richter, A., and Burrows, J. P.: Systematic analysis of interannual and seasonal variations of model-simulated tropospheric NO_2 in Asia and comparison with GOME-satellite data, Atmos. Chem. Phys., 7, 1671–1681, doi:10.5194/acp-7-1671-2007, 2007.

Valin, L. C., Russell, A. R., Hudman, R. C., and Cohen, R. C.: Effects of model resolution on the interpretation of satellite NO_2 observations, Atmos. Chem. Phys., 11, 11647–11655, doi:10.5194/acp-11-11647-2011, 2011.

van Noije, T. P. C., Eskes, H. J., Dentener, F. J., Stevenson, D. S., Ellingsen, K., Schultz, M. G., Wild, O., Amann, M., Atherton, C. S., Bergmann, D. J., Bey, I., Boersma, K. F., Butler, T., Cofala, J., Drevet, J., Fiore, A. M., Gauss, M., Hauglustaine, D. A., Horowitz, L. W., Isaksen, I. S. A., Krol, M. C., Lamarque, J.-F., Lawrence, M. G., Martin, R. V., Montanaro, V., Müller, J.-F., Pitari, G., Prather, M. J., Pyle, J. A., Richter, A., Rodriguez, J. M., Savage, N. H., Strahan, S. E., Sudo, K., Szopa, S., and van Roozendael, M.: Multi-model ensemble simulations of tropospheric NO_2 compared with GOME retrievals for the year 2000, Atmos. Chem. Phys., 6, 2943–2979, doi:10.5194/acp-6-2943-2006, 2006.

Wild, O. and Prather, M. J.: Global tropospheric ozone modeling: quantifying errors due to grid resolution, J. Geophys. Res., 111, D11305, doi:10.1029/2005JD006605, 2006.

Table 1. Conditions for sensitivity simulations by CMAQ.

Run #	Horizontal resolution (km)	Number of vertical layer	Emission strength	Soil-NO_x emission	Injection height	Diurnal variation
1	80	37	–	on	–	–
2	40	37	–	on	–	–
3	20	37	–	on	–	–
4	10	37	–	on	–	–
5	80	37	+20 %	on	–	–
6	80	37	−20 %	on	–	–
7	80	37	–	off	–	–
8	80	14	–	on	–	–
9	80	37	–	on	reduced by half	–
10	80	37	–	on	–	turned on

Table 2. Twelve diagnostic regions selected for this work.

	Name	Longitude (° E)		Latitude (° N)	
CEC	Central Eastern China	110.0	123.0	30.0	40.0
NCP	North China Plain	113.0	117.5	34.0	39.0
BEI	Beijing	115.5	117.5	39.0	41.0
SCN[a]	Sichuan	103.5	107.5	27.5	31.5
YTD	Yangtze Delta	117.5	122.5	30.0	34.0
PRD[a]	Pearl River Delta	111.0	115.0	21.5	25.0
JPN	Japan	133.0	141.0	33.5	37.0
KOR	Korea	125.0	130.0	34.5	39.0
ECS	East China Sea	125.0	129.5	29.0	33.0
SOJ	Sea of Japan	130.0	138.0	37.0	40.5
SCS	South of East China Sea	125.0	129.5	25.0	28.0
SJP	South of Japan	132.0	138.0	28.0	32.0

[a] Out of range for the 10 km resolution domain (Fig. 1).

Table 3. Ratios of CMAQ-simulated tropospheric NO_2 VCD values at horizontal resolutions of 10 and 80 km.

	June			December		
	09:30 LT	10:00 LT	13:45 LT	09:30 LT	10:00 LT	13:45 LT
CEC	1.15	1.18	1.28	1.18	1.19	1.19
NCP	1.18	1.21	1.33	1.21	1.21	1.21
BEI	1.48	1.55	2.06	1.46	1.47	1.47
SCN[a]	(1.13)	(1.15)	(1.13)	(1.18)	(1.19)	(1.26)
YTD	1.11	1.13	1.29	1.18	1.18	1.18
PRD[a]	(1.35)	(1.41)	(1.44)	(1.20)	(1.21)	(1.30)
JPN	1.30	1.36	1.62	1.12	1.12	1.11
KOR	1.28	1.34	1.55	1.11	1.11	1.14
ECS	1.15	1.17	1.15	1.54	1.55	1.67
SOJ	1.03	1.07	1.05	1.10	1.11	1.17
SCS	1.17	1.22	1.32	1.34	1.37	1.42
SJP	1.09	1.11	1.12	1.47	1.47	1.67

[a]Ratios of tropospheric NO_2 VCDs at horizontal resolutions of 20 and 80 km.

Table 4. Tropospheric NO_2 VCD values derived from satellite observations (10^{15} molecules cm^{-2}). a.m. values are averages of VCDs at 09:30 (GOME-2) and 10:00 (SCIAMACHY). p.m. values are from VCDs at 13:45 (OMI).

	June			December		
	a.m. VCD	p.m. VCD	p.m./a.m.	a.m. VCD	p.m. VCD	p.m./a.m.
CEC	10.1	5.9	0.58	30.2	16.9	0.56
NCP	16.7	8.9	0.53	58.9	27.7	0.47
BEI	18.0	10.3	0.57	41.6	23.6	0.57
SCN	5.3	3.0	0.57	13.5	6.9	0.51
YTD	12.9	5.9	0.46	21.2	15.8	0.75
PRD	7.3	3.3	0.42	9.7	9.0	0.93
JPN	4.7	3.4	0.72	7.6	6.7	0.88
KOR	5.8	4.3	0.74	8.3	5.4	0.65
ECS	1.0	1.0	1.00	1.8	1.3	0.72
SOJ	1.1	1.1	1.00	0.1	0.4	4.00
SCS	0.7	0.6	0.86	0.7	0.9	1.29
SJP	0.7	0.6	0.86	1.3	1.2	0.92

Table 5. Tropospheric NO_2 VCD values derived from CMAQ simulations (10^{15} molecules cm^{-2}). a.m. values are averages of VCDs at 09:30 and 10:00. p.m. values are from VCDs at 13:45.

	June			December		
	a.m. VCD	p.m. VCD	p.m./a.m.	a.m. VCD	p.m. VCD	p.m./a.m.
CEC	8.5	5.7	0.67	21.0	21.8	1.04
NCP	14.1	8.8	0.62	32.0	31.6	0.99
BEI	12.2	7.3	0.60	20.3	20.8	1.02
SCN	5.0	3.1	0.62	8.4	7.8	0.93
YTD	11.1	7.6	0.68	20.6	22.3	1.08
PRD	4.1	2.3	0.56	7.6	5.7	0.75
JPN	4.3	2.7	0.63	7.7	7.7	1.00
KOR	4.2	2.8	0.67	10.3	10.3	1.00
ECS	1.2	0.9	0.75	2.7	2.5	0.93
SOJ	1.1	0.8	0.73	3.7	3.7	1.00
SCS	0.9	0.7	0.78	1.6	1.3	0.81
SJP	0.9	0.7	0.78	2.2	1.9	0.86

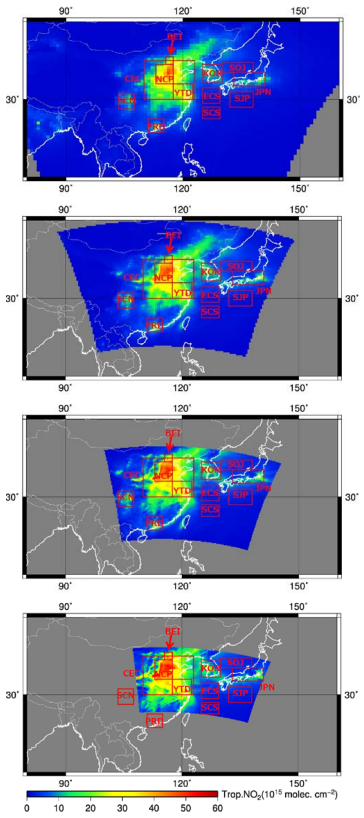

Fig. 1. Twelve selected diagnostic rectangular regions superimposed on a map of CMAQ tropospheric NO_2 columns at 80, 40, 20, and 10 km horizontal resolutions.

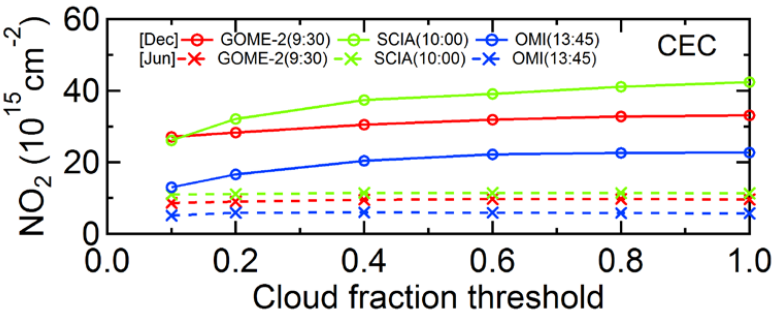

Fig. 2. Dependence of satellite-based tropospheric NO_2 VCDs on the choice of cloud fraction threshold over the CEC region.

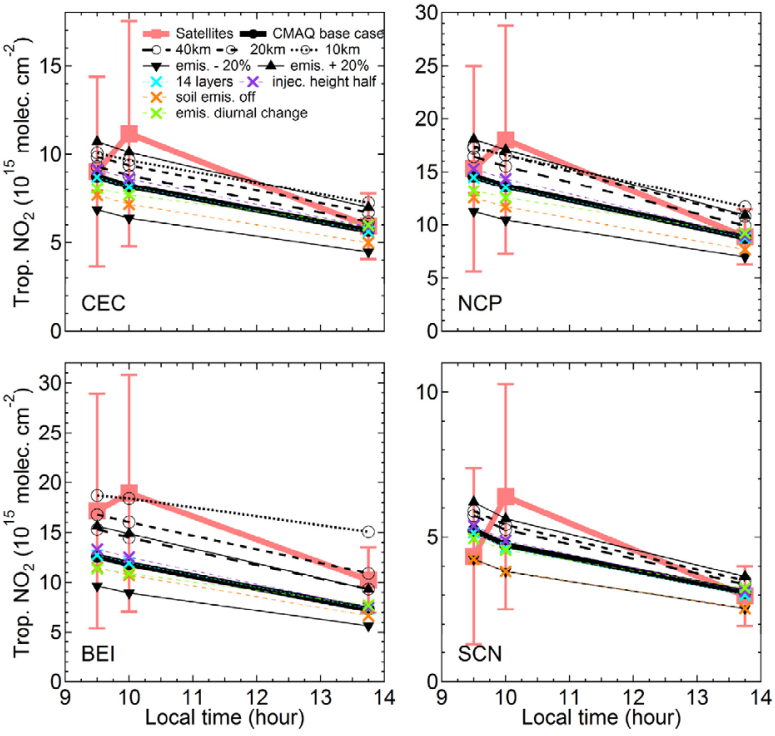

Fig. 3. Comparisons for the CEC, NCP, BEI, and SCN regions in June 2007.

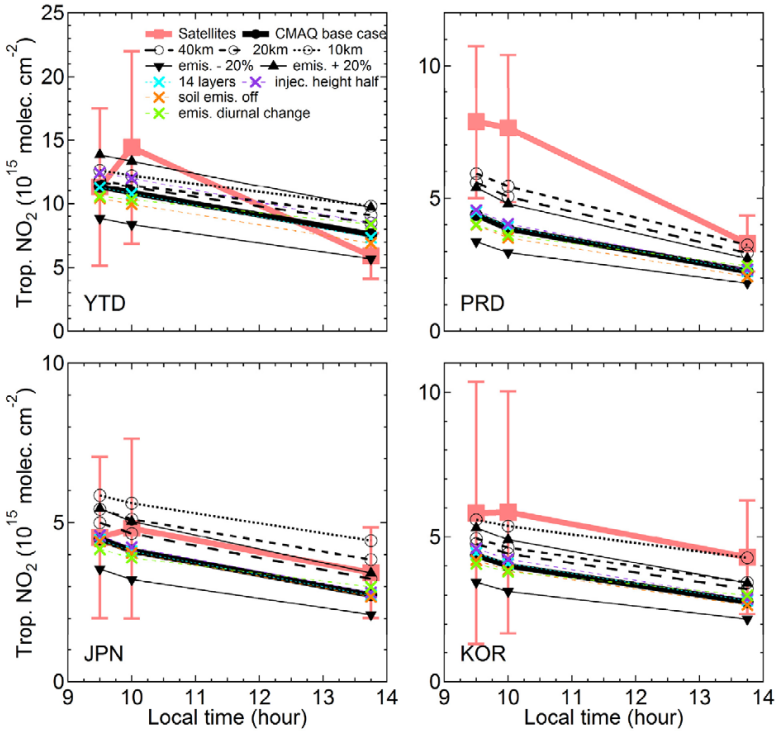

Fig. 4. Comparisons for the YTD, PRD, JPN, and KOR regions in June 2007.

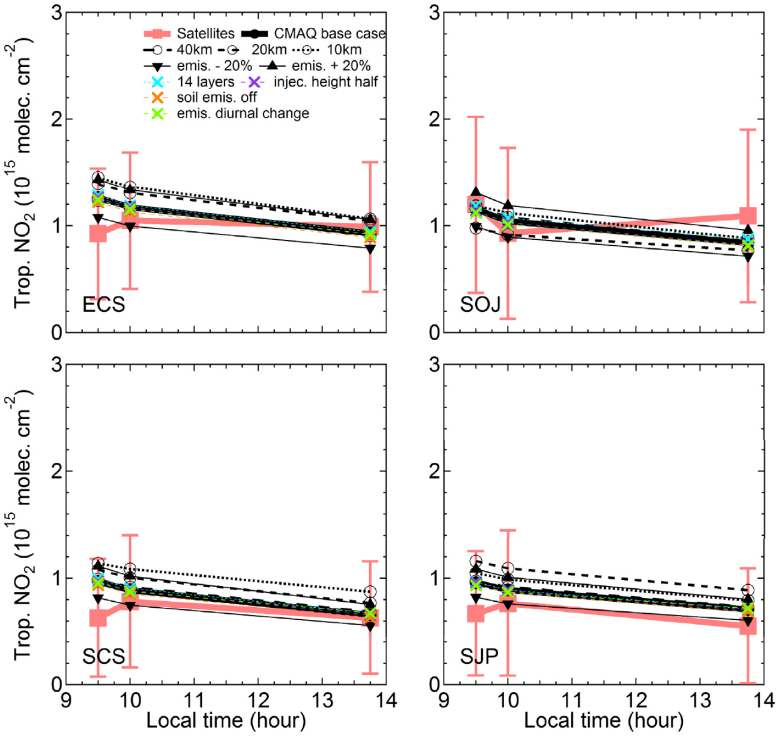

Fig. 5. Comparisons for the ECS, SOJ, SCS, and SJP regions in June 2007.

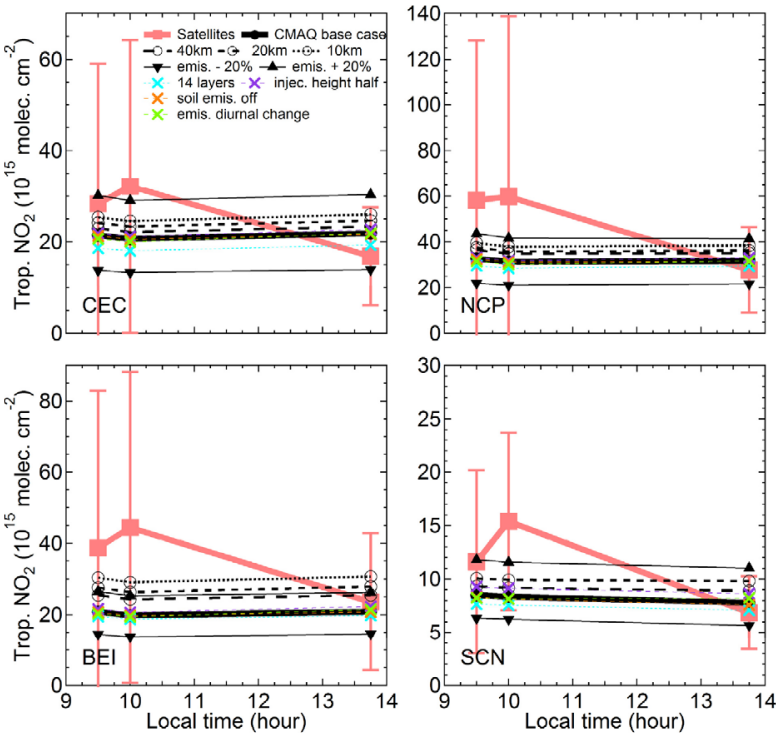

Fig. 6. Comparisons for the CEC, NCP, BEI, and SCN regions in December 2007.

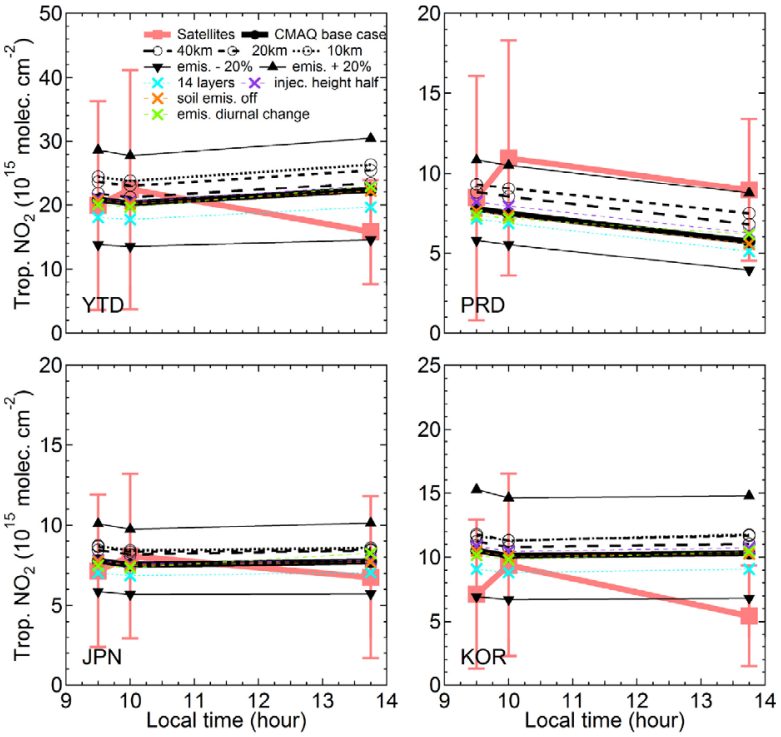

Fig. 7. Comparisons for the YTD, PRD, JPN, and KOR regions in December 2007.

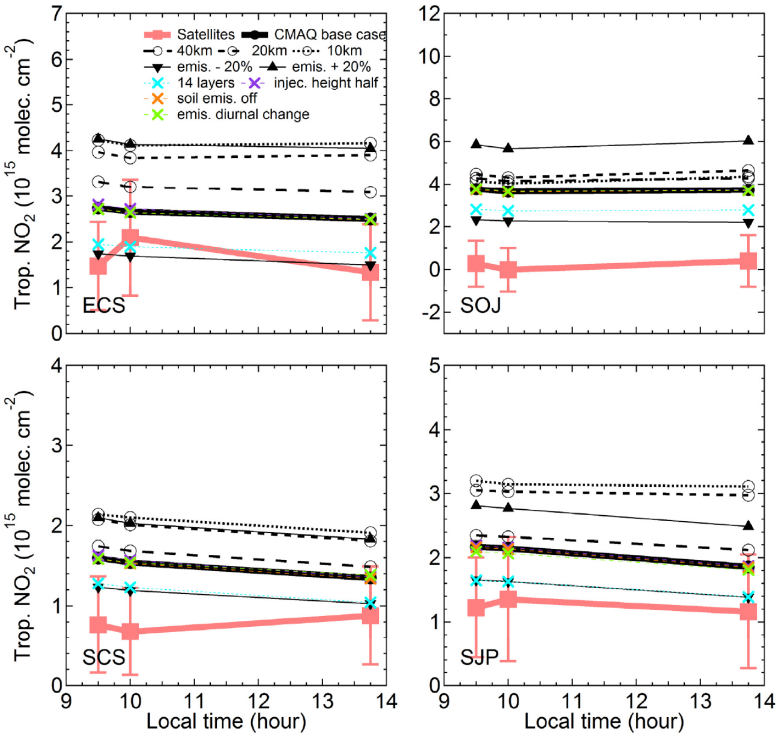

Fig. 8. Comparisons for the ECS, SOJ, SCS, and SJP regions in December 2007.